An Insight into Evolution of Light Weight High Entropy Alloys: A Review

Amit Kumar and Manoj Gupta *

Department of Mechanical Engineering, National University of Singapore, 9 Engineering Drive 1, Singapore 117576, Singapore; amittonk@gmail.com
* Correspondence: mpegm@nus.edu.sg; Tel.: +65-6516-6358

Abstract: High Entropy Alloys (HEAs) are the most recently developed new class of materials, which are known for their unique structural properties. Lightweight materials are currently in excessive demand for transportation and energy saving applications. In this review, efforts have been made to summarize the work done towards the development of HEAs targeting lightweight applications. Some new synthesis techniques are suggested for the fabrication of lightweight HEAs (LWHEAs). The concept of porous structure fabrication, microwave sintering of green compact, casting by disintegration melt deposition and advanced manufacturing using additive manufacturing are discussed as future directions of LWHEAs synthesis. LWHEAs for potential biomedical applications have also been addressed.

Keywords: lightweight high entropy alloy; porous structure; disintegrated melt deposition; microwave sintering

1. Introduction

Development of lightweight materials for industrial applications is one of the challenging research areas in the present scenario. Aviation, automobile and whole energy sector is highly dependent on the research progress in this area in order to replace high-density metals and alloys with new lightweight materials without compromising on structural properties and no significant rise in cost [1]. In transportation sector, there is a high emphasis on greenhouse gas reductions and improving fuel efficiency. The weight reduction is still the most cost-effective means to reduce fuel consumption and greenhouse gases emissions for the transportation sector. It has been calculated that for every 10% of weight reduction in total weight of a vehicle there is 7% reduction in fuel consumption, which means that there is about 20 kg of carbon dioxide reduction for every kilogram of weight reduced in a vehicle [2]. The main drawback of the existing lightweight materials is either their limited properties or high manufacturing cost. Thus, continuous efforts are being made by researchers to develop new types of lightweight alloys, which are low in cost and capable of meeting properties requirements [3]. Over past three decades, efforts have been made to replace steel and iron with aluminium, magnesium and composites based materials. Multicomponent alloys (HEAs) have shown promising properties and are investigated for lightweight applications.

Development of HEAs is one of the breakthroughs in the direction of development of new class of material, which opened new possibilities for development of a vast number of unique materials [4–12]. HEAs have been investigated recently to obtain the combination of good structural properties such as high hardness (100 to 1100 Hv) [12], work hardening capacity, wear resistance [9], high-temperature precipitation hardening (600 to 1000 °C), anti-oxidation and anti-corrosion resistance [9–11]. HEAs are fundamentally different from the traditionally developed alloys in such a way that it has a significantly high amount of mixing entropy, which enhances the stability of solid solution compared to intermetallic

compounds, especially at high temperatures. HEAs generally contain at least five principal elements, each having atomic percentage between 5% and 35% [4,13]. HEAs have been shown to possess a comparatively simplified structure with extraordinary properties. Most of the alloys consist majority of solid solution phases together with small amounts of intermetallic compounds [14].

Because of their extraordinary properties, HEAs are suitable for numerous industrial applications [13]. For example, CoCrFeMnNi alloy is very suitable for cryogenic applications (liquefied gas storage) as it can retain mechanical properties at a temperature as low as 77 K [15]. Because of anticorrosion, anti-oxidation and wear resistance properties, HEAs coatings can be used in food preservation and cooking ware [16]. HEAs can be used to suppress electromagnetic interference, especially in electronics. AlCoFeNiTi and CoCrFeNiTi systems of alloy exhibit good binding properties and can be used as hard metals alloy binders [17]. Powder of HEAs are being coated on the surface of tools, dies, nozzles and molds by thermal-spray or plasma arc [16]. HEAs can be used to protect the surface of machine components and tools because of their high hardness, wear resistance, high-temperature softening resistance, anti-corrosion, and combinations of these properties [14,18,19]. This clearly indicates a wider scope for the application of high entropy alloys.

Initially, HEAs were developed for high-temperature refractory applications to replace the super alloys [20–22]. Therefore, most of the HEAs compositions exhibit high-density values of more than 10 g·cm^{-3}. For its applications in transportation, energy and biomedical sectors, alloys with lower densities and higher strengths are required. Thus far, there are only a few investigations made on the fabrication of low-density HEAs. Senkov et al. designed Cr-Nb-Ti-V-Zr refractory alloy system to lower the density of HEA to approximately 6.49 g·cm^{-3} in order to create lightweight materials with high strength even at a higher temperature (1000 °C) [23,24]. However, this density value is significantly higher and needs to further reduce for lightweight applications. In another effort made by Stepanov et al., heavy Cr was replaced with Al in Al$_x$NbTiVZr refractory alloys and density was lowered to 5.55 g·cm^{-3} [25]. However, this was also much higher than the 3 g·cm^{-3} that material selectors look for in lightweight materials. Juan et al. [26] synthesized Al$_{20}$Be$_{20}$Fe$_{10}$Si$_{15}$Ti$_{35}$ alloy by casting method, which exhibited a density of 3.91 g·cm^{-3} and as-cast microstructure composed of one major and two minor phases. Li et al. [27,28] also prepared HEA containing Mg with a composition of Mg$_x$(AlCuMnZn)$_{100-x}$ using induction melting and casting route. The alloys exhibited multi-phase structure, composed mainly of hcp phases and Al-Mn icosahedral quasicrystalline phases. Depending on the percentage of Mg in composition, the alloys exhibited densities in the range of 2.20–4.29 g·cm^{-3}. These alloys exhibited good compressive strengths (400–500 MPa) at room temperature but ductility values were about 3% to 5% in compression. Similar microstructures and mechanical properties were subsequently observed in the equiatomic systems that were cast and cooled in air, water or brine solutions [28]. Chen et al. used mechanical alloying to prepare BeCoMgTi and BeCoMgTiZn, but both the alloys formed resulted in amorphous phase [29]. Youssef et al. reported low density (2.67 g·cm^{-3}), high hardness HEA with close-packed single-phase nanocrystalline structure with the actual composition of Al$_{20}$Li$_{20}$Mg$_{10}$Sc$_{20}$Ti$_{30}$ using mechanical alloying technique [30]. Thus, the results of literature search revealed that there are only two compositions, Mg$_x$(AlCuMnZn)$_{100-x}$ and Al$_{20}$Li$_{20}$Mg$_{10}$Sc$_{20}$Ti$_{30}$, that show density level below 3 g·cm^{-3} and can be classified as lightweight HEAs.

Accordingly, in this review paper, the main focus has been given to summarize the efforts made to develop low-density high entropy alloys or lightweight high-entropy alloys (LWHEAs), basic principles of HEA designing, thermodynamic parameters of solid solution formation, and deviation from the equiatomic composition to develop single phase stable structure. In addition, theoretical aspects of LWHEA designing have been discussed using a non-equiatomic composition as an example. Processing routes used for fabrication, microstructural and mechanical characterization of LWHEAs has also been discussed. Further, the future direction of manufacturing LWHEA using the concept of porous structures has also been suggested to lower the density of already developed HEAs targeting biomedical, automobile and aviation applications.

2. Basic Principles of LWHEA Designing

In general, the basic principles of designing LWHEA are the same as that for HEAs except the selection of principle alloying elements, which decide the density of that alloy. For making this review more understandable, a brief summary of designing principles discussed in this section.

From statistical thermodynamics, configurational entropy of a single phase system can be given by Boltzmann's equation [31]:

$$\Delta S_{\mathrm{conf}} = -k\mathrm{ln}w \tag{1}$$

where k is Boltzmann's constant and w is the number of ways in which the available energy can be mixed or shared among the particles of the system. If there are n elements with c_i mole fraction, then Equation (1) converts to:

$$\Delta S_{\mathrm{conf}} = -R \sum_{i=1}^{n} c_i \mathrm{ln}c_i \tag{2}$$

For an equiatomic alloy, configurational entropy per mole can be expressed as [4,32]:

$$\Delta S_{\mathrm{conf}} = -k\mathrm{ln}w = -R\mathrm{ln}\frac{1}{n} = R\mathrm{ln}n \tag{3}$$

where R is the gas constant, 8.314 J/K mol.

From Equation (3), ΔS_{conf} for an alloy having five elements is given as R ln5 = 1.61R. It has been defined that if the $\Delta S_{\mathrm{conf}} \geq 1.5R$ the alloys formed will be considered high entropy alloys [33]. Most of the super alloys, either Ni-base or Co-base, are low entropy alloys as $\Delta S_{\mathrm{conf}} < 1R$, whereas BMGs (bulk metallic glasses) exhibit medium entropy between 1R to 1.5R. Hence, none of the traditional alloys have mixing entropy higher than 1.5R.

From Equation (1), it is also clear that an element having a concentration of 5 at % will contribute 0.15R to mixing entropy, which is just 10% of the minimum requirement of 1.5R for HEAs. Therefore if we have five elements in equiatomic concentration, then this requirement can be achieved [33].

2.1. Core Effects of HEA

There are four core effects on which the microstructure and properties of HEAs depend [33]: high entropy, severe lattice distortion, sluggish diffusion, and cocktail effects [32,33]. For the thermodynamics of solid solution formation, *High-entropy effect* is the important effect. Due to this effect, the microstructure of HEA is much simpler than expected. Gibbs free energy of mixing, ΔG_{mix}, is a function of enthalpy of mixing (ΔH_{mix}) and entropy of mixing (ΔS_{mix}). If the number of elements is higher in an alloy, the ΔG_{mix} will be lower, as the ΔS_{mix} contribution will be large, especially at high temperatures. Therefore, the higher is the entropy of configuration, the lower is the energy of the random solid solution phase and simpler is the microstructure formed at equilibrium.

For better structural properties, *severe lattice distortion effect* is responsible to an extent. Compared to one element dominating alloy, lattice distortion in HEA is severe because each element atom is different in size and has the same probability of occupying the lattice site. This effect not only affects the various properties but also reduces the thermal effect on properties. Due to large solution hardening, hardness and strength effectively increase in severely distorted HEA lattice.

For the stability of phase and kinetics of phase transformation, *sluggish diffusion effect* is responsible in HEAs. Formation of new phases requires diffusion to occur between different atoms present in the microstructure. As HEAs mainly contain a random solid solution, and or ordered solid solution, their matrices are considered as whole-solute matrices. Diffusion of an atom in a whole-solute matrix is extremely difficult, as a vacancy in the whole-solute matrix is surrounded by different-element atoms during diffusion. It has been proposed that slower diffusion and higher activation energy would occur in HEAs due to the larger fluctuation of lattice potential energy (LPE) between lattice sites [34]. The abundant low-LPE sites can serve as traps and hinder the diffusion of atoms. This leads to the sluggish diffusion effect.

In HEAs, *cocktail effect* is used to emphasize the enhancement of the properties by at least five major elements. Each phase is a multicomponent solid solution and can be considered as an atomic-scale composite. Its composite properties not only come from the basic properties of elements by the mixture rule but also from the mutual interactions among all the elements and from the severe lattice distortion. Mutual interaction and lattice distortion would bring excess quantities in addition to those predicted by the mixture rule.

2.2. Thermodynamic Parameters for the Formation of Solid Solution and Metallic Glass

Some thermodynamic parameters have been used to define the conditions for the formation of BMG or a solid solution in multicomponent alloys such as ΔH_{mix}, ΔS_{mix} and topological parameters like δ [35,36]. Zhang et al. [36] have shown that simple solid solutions will form in alloys if $-20 \leq \Delta H_{\text{mix}} \leq 5$ kJ/mol, $12 \leq \Delta S_{\text{mix}} \leq 17.5$ J/K mol, and δ ≤ 6.4%. When only disordered phases are allowed, the criteria are more restrictive, requiring a smaller negative limit of ΔH_{mix} (≥ -15 kJ/mol) and a smaller δ (≤4.6%). Here δ is defined as [36]:

$$\delta = 100 \sqrt{\sum_{i=1}^{n} c_i \left(1 - \frac{r_i}{\bar{r}}\right)^2} \tag{4}$$

where c_i and r_i are compositions and atomic radii of *i*th element and $\bar{r}$ is the average atomic radius. Later, another thermodynamic parameter Ω was also introduced for the prediction of solid solution formation as [37,38]:

$$\Omega = \frac{T_m \Delta S_{\text{mix}}}{|\Delta H_{\text{mix}}|} \tag{5}$$

where $T_m = \sum_{i=1}^{n} c_i (T_m)_i$ is the hypothetical melting temperature calculated according to the rule of mixtures. Thus, the new criteria for simple solid solutions formation are when $\Omega \geq 1.1$ and δ ≤ 6.6% [37].

Guo et al. [39] suggested that all parameters ΔH_{mix}, δ and ΔS_{mix} should be used to identify solid solution formation. They suggested if $-22 \leq \Delta H_{\text{mix}} \leq 7$ kJ/mol, $0 \leq \delta \leq 8.5$, and $11 \leq \Delta S_{\text{mix}} \leq 19.5$ J/K·mol, then only the solid solution HEA will form. If $-49 \leq \Delta H_{mix} \leq 25.5$ kJ/mol, $\delta \geq 9$, and $7 \leq \Delta S_{\text{mix}} \leq 16$ J/K·mol, then BMG will form. Guo et al. [39] also reported that the valence electron concentration (VEC) is the critical parameter for the determination of BCC and FCC phase formation in HEAs. FCC phase forms when VEC ≥ 8, whereas BCC phase forms when VEC < 6.87. FCC and BCC coexist in between. This criterion is interesting since the FCC stabilizers or formers such as Co and Ni have VEC = 9 and 10, respectively, whereas BCC stabilizers such as Al and Ti have VEC = 3 and 4, respectively. That implies that more FCC elements tend to form FCC phase.

2.3. Non-Equiatomic Composition as a Better Design Approach

The principle of designing HEAs is based on maximization of configurational entropy (CE) in order to reduce Gibbs free energy [4], which results in phases with simple structures, rather than brittle ordered intermetallics [40–42]. This is the reason HEAs were initially defined to consist of at least five principal elements of concentrations between 5 and 35 at %, in order to maximize the CE and facilitate the formation of solid solutions. However, many recent investigations have raised questions on such a dominant role of the CE independent of the mixing enthalpy, and it has stressed that the Gibbs free energy is a dominating parameter for phase formation, even in cases of increased CE [43,44]. Even though the role of the CE is still not very clear, the majority of the investigated HEAs still follow the near-equiatomic ratios. Few non-equiatomic HEAs systems have been investigated to date. Microstructural characterization results increasingly reveal that most of the HEAs that have been studied so far are actually not single-phase materials but often contain intermetallic phases [43,45–47]. The presence of intermetallic phases typically deteriorates most of the key mechanical properties such as ductility, fatigue resistance, and toughness. Alloys containing intermetallic phases, therefore, often

reveal inferior properties compared to corresponding single-phase alloys of similar, yet non-equiatomic composition [48].

Recently, Tasan et al. [48,49] showed that the equiatomic quaternary CoCrFeMn alloy surprisingly leads to a complex multiphase microstructure containing several intermetallic phases, while the non-equiatomic material $Co_{10}CrFe_{40}Mn_{10}$ produces a homogeneous fcc single phase. In some other work done by the same group [50], a novel single phase, non-equiatomic CoCrFeMnNi high-entropy alloy with exceptional phase stability and tensile ductility is reported. These reports show that the high entropy contribution alone is not sufficient to stabilize the matrix and to over-compensate enthalpy advantages of competing intermetallic phases. Authors suggested that this might be the reason why only few compositions of HEAs could truly achieve single-phase structure. To produce a homogeneous single phase crystalline solid solutions, it is more important to avoid the formation of intermetallic phases rather maximize the entropy [43,44,49,50]. Therefore, from a thermodynamic point of view, it is more important to analyze the likelihood of intermetallic compounds in the multi-component phase diagram rather than only analyzing the configurational entropy.

Rabbe et al. [51] recently reported high-entropy steels designed on the basis of non-equiatomic matrix elements Fe, Mn, Ni, C, N, and Co. This showed a single phase solid solutions with face-centered cubic crystal structure. Authors explained that this observation is due to the fact that in many transition metal alloy solid solutions, the shape of the configurational entropy as a function of chemical composition assumes a relatively flat and compositionally wide plateau. This means that the entropy curve has a weak maximum and no steep changes, except for the case of very small concentrations [48]. This fact suggests that entropy-based stabilization of massive solid solutions can also be achieved for non-equiatomic quinary and quaternary alloy compositions [48–50]. This modifies the original high entropy alloying concept, where none of the alloying elements were meant to dominate. Another benefit given for designing non-equiatomic compositionally simplified high-entropy alloys is to reduce the alloying costs. Any material beyond a certain critical amount, if not contributing to the desired properties of alloy, needs to be reduced in its content. In addition, it may be noted that non-equiatomic compositions exhibit reducing variations in vapor pressure, typically occurring in multi-component systems, cause less segregation, and improved casting properties. Thus, introducing a non-equiatomic mixing rule would provide a much larger compositional space for synthesizing lightweight high entropy alloys without intermetallic phases.

2.4. Theoretical Aspects and Designing of a LWHEA

For a multi-component alloy, it is more difficult to construct its phase diagram. In such condition, besides just theoretical modeling [35,38,52–54], computational approaches, such as density functional theory (DFT) calculations [55] and ab initio molecular dynamics (AIMD) [56] simulations, can also be used to study phase formation in HEAs. Due to the significant cost and computational time required based on the current technology and among other limitations [17], these approaches are not feasible for designing of HEAs. Rather, a semi-empirical computational approach, known as calculations of phase diagrams (CALPHAD), can be used to predict equilibrium phases in HEAs [56–59]. CALPHAD can predict the equilibrium phase(s) of a multicomponent system based on the existing data obtained from binary and ternary systems, by directly computing the minimum Gibbs free energy at a given temperature and pressure [59,60]. Ye et al. [61] have already reported that the predictions from both the CALPHAD calculation and the phase parameter (ψ) are in general agreement with the experimental results of single-phase solid solutions. Recently, Gao et al. [62] also performed CALPHAD calculation for the formation of HEAs containing HCP solid solution. However, a few exceptional cases were noted from among the alloys containing Fe-Cu, such as CoCrCuFeNi and CrCuFeMoNi [63]. This is due to the fact that Fe and Cu physically hold a positive enthalpy of mixing and in combination, they are likely to cause elemental segregation inducing local precipitations [64].

To get a deep insight in theoretical calculations of designing a LWHEA, an example of a multi-component system is being considered. Here, we consider an alloy of non-equiatomic

composition $Al_{35}Li_{20}Mg_{35}Ti_5Zn_5$ for exploring its theoretical possibility to be a LWHEA. It should be noted that this alloy example considered here is to just illustrate the theoretical design aspects and there are no experimental results available for this alloy in the literature. Table 1 lists the various thermodynamic and physical properties of different elements of $Al_{35}Li_{20}Mg_{35}Ti_5Zn_5$ alloy. Overall density calculation shows that this alloy belongs to the LWHEA category as value is 3.00 gm/cc. Some previous reports [65–67] have shown that in multi-component HEAs, intermetallic compounds and amorphous phases may also form besides solid-solutions phases, while, owing to the promising properties in multi-component HEAs, simple solid-solution phases are the most expected to form [4,68].

In order to predict the solid-solution formation rule in multi-component alloys, Gibbs free energy for multi-component alloy systems has been considered an important parameter. However, for multi-component systems, it is difficult to calculate ΔG accurately at a certain composition and temperature. Takeuchi and Inoue [69] have proposed an assumption for multi-component alloy systems—ΔG at a certain composition is proportional to the free energy of mixing ΔG_{mix} of the liquid phase—and successfully utilize it to calculate critical cooling rate for metallic glasses. In this calculation, this assumption has also been adopted. Free energy of mixing ΔG_{mix} can be expressed as:

$$\Delta G_{\text{mix}} = \Delta H_{\text{mix}} - T\Delta S_{\text{mix}} \tag{6}$$

where T is the absolute temperature, ΔH_{mix} is the enthalpy of mixing and ΔS_{mix} is the entropy of mixing. For the considered example, a regular solid solution model has been considered to simplify the calculation for free energy of multi-component HEAs.

Therefore, enthalpy of mixing for $Al_{35}Li_{20}Mg_{35}Ti_5Zn_5$ alloy with five elements can be determined from Equation (7):

$$\Delta H_{\text{mix}} = \sum_{i=1,\ i\neq j}^{5} \Omega_{ij} c_i c_j \tag{7}$$

where $\Omega_{ij} \left(= 4\Delta H_{AB}^{mix}\right)$ is the regular solution interaction parameter between the *i*th and *j*th elements. For the calculation, the values of enthalpy of mixing $4\Delta H_{AB}^{mix}$ on the basis of Miedema macroscopic model for binary liquid alloys is obtained from the Ref. [70]. Table 1 shows the various thermodynamic properties of the $Al_{35}Li_{20}Mg_{35}Ti_5Zn_5$ alloy for theoretical calculations.

Table 1. Various thermodynamic and physical properties of different elements used in multi-component alloy.

Elements	Mole Fraction (c_i)	Atomic Radius (*r*)	Density (g/cc)	Two Elements	$\Delta H_{\langle ij \rangle}^{\text{mix}}$ (kJ/mol)	Two Elements	$\Delta H_{\langle ij \rangle}^{\text{mix}}$ (kJ/mol)
Mg	0.35	160	1.74	Mg, Li	−0.33	Li, Ti	34.854
Li	0.2	151	0.53	Mg, Al	−1.662	Li, Zn	−6.893
Al	0.35	143	2.7	Mg, Ti	13.542	Al, Ti	−40.481
Ti	0.5	146	4.51	Mg, Zn	−3.445	Al, Zn	0.637
Zn	0.5	142	7.14	Li, Al	−3.384	Ti, Zn	−22.324

Substituting the values of various enthalpy of mixing into Equation (7):

$$
\begin{aligned}
\Delta H_{\text{mix}} = 4\times \quad & \{(-0.33 \times 0.35 \times 0.2) + (-1.662 \times 0.35 \times 0.35) \\
& + (13.542 \times 0.35 \times 0.05) + (-3.445 \times 0.35 \times 0.05) \\
& + (-3.384 \times 0.2 \times 0.35) + (34.854 \times 0.2 \times 0.05) \\
& + \ (-6.893 \times 0.2 \times 0.05) + (-40.481 \times 0.35 \times 0.05) \\
& + (0.637 \times 0.35 \times 0.05) + \ (-22.324 \times 0.05 \times 0.05)\} \\
& = -3.041 \text{ KJ/mol}
\end{aligned}
$$

Thus, ΔH_{mix} obtained for the alloy is within the range ($-22 \leq \Delta H_{\text{mix}} \leq 7$ kJ/mol) defined for the formation of HEA. The negative ΔH_{mix} is inclined to make the different elements combine to be

intermetallic compound. Moreover, the more negative ΔH_{mix} means the larger binding force between elements. The more positive ΔH_{mix} means the less miscibility of the different elements in the liquid alloy, which leads to separation or segregation of different elements in alloy. Whatever the sign of ΔH_{mix} is, the larger absolute value of ΔH_{mix} will make solid-solution hardly form. Only when the value of ΔH_{mix} is close to zero, the different elements can randomly distribute in the alloy, and the solid-solution phases can stably occur in the solid phase. This is consistent with the experimental results in Reference [71].

Another parameter is entropy of mixing, which, according to Boltzmann's hypothesis, for five-element regular solution is given as:

$$\Delta S_{\text{mix}} = -R \sum_{i=1}^{5} (c_i \ln c_i) \tag{8}$$

where c_i is mole percent of component, $\sum_{i=1}^{n} c_i = 1$, and R (8.314 J K^{-1} mol^{-1}) is gas constant. Substituting the values into Equation (8):

$$\begin{aligned}\Delta S_{\text{mix}} = -8.314 \quad &\times \{(0.35 \times \ln 0.35) + (0.1 \times \ln 0.1) + (0.35 \times \ln 0.35) \\ &+ (0.15 \times \ln 0.15) + (0.05 \times \ln 0.05)\} = \frac{11.277 \text{ J}}{\text{K.mol}}\end{aligned}$$

Thus, ΔS_{mix} entropy of mixing is also within the range ($11 \leq \Delta S_{\text{mix}} \leq 19.5$ J/K mol) defined for the formation of HEA. For the equiatomic alloy, the entropy of mixing would be the maximum. Therefore, equal/near-equal atomic ratio multi-component HEAs have much higher entropy of mixing than conventional alloys. The value of ΔS_{mix} is always positive in multi-component alloy. The high ΔS_{mix} can effectively increase the extent of confusion in alloy system and significantly lower ΔT_{mix}, thus the different elements would randomly distribute in the crystal lattice and the tendency of ordering and segregation of alloy elements is lowered by the high ΔS_{mix}. Consequently, the high ΔS_{mix} can make random solid-solution form easily and more stable than intermetallic compounds or other ordered phases during solidification in alloys.

In addition, the effect of ΔS_{mix} becomes more and more prominent as the temperature increases. Therefore, the large value of $T\Delta S_{\text{mix}}$ would facilitate forming solid-solutions. It implies that the effect of the HE of mixing could balance the effect of the enthalpy of mixing for forming solid-solution at certain temperature; that is, the driving force is equal to the resistance. Ignoring the solid-state phase transition, the phase formation generally occurs near the melting temperature (T_m) of alloy. Hence, T_m is adopted for the entropy term $T\Delta S_{\text{mix}}$, and a parameter Ω is defined for predicting the solid-solution formation for various multi-component alloys. The melting temperature of five-elements alloy, T_m, is calculated using the rule of mixtures:

$$T_m = (0.35 \times 923.2) + (0.2 \times 180.5) + (0.35 \times 933.5) + (0.05 \times 1941) + (0.05 \times 692.7)$$
$$T_m = 817.63 \text{ K}$$

Substituting the various values of enthalpy, entropy and temperature into Equation (5):

$$\Omega = \frac{T_m \Delta S_{\text{mix}}}{|\Delta H_{\text{mix}}|} = \frac{817.63 \times 11.277}{3.041 \times 1000} = 3.032$$

If $\Omega > 1$, the contribution of $T\Delta S_{\text{mix}}$ will exceed that of ΔH_{mix} for solid-solution formation, and the multi-component HEAs are mainly composed of the solid solutions. Thus, the value of Ω for this alloy indicates the solid-solution formation ability.

Even though the value of Ω clearly indicates the formation of solid solution, the atomic size mismatch effect is also an important criterion. In multi-component HEAs, owing to the similar concentration of elements, all atoms are expected to randomly occupy the crystal lattice sites on the basis of a statistical average probability of occupancy. Therefore, each component element can

be regarded as the solute element for forming solid solution. Large atomic size difference between elements cause serious lattice distortion in alloy and the corresponding free energy will increase, which could lower the stability of solid-solution. On the other hand, significant difference in atomic size ratios could lead to the sluggish diffusion of atoms in the matrix, which lowers the phase transformation rate and makes the atoms segregate in the alloy, even causes nanocrystalline and amorphous structures to form. For the considered alloy, the average size $\bar{r}$ can be calculated as:

$$\bar{r} = \frac{(160 + 151 + 143 + 146 + 142)}{5} = 148.4$$

Substituting the various atomic radius size from Table 1 into Equation (4):

$$\delta = 100 \times \left\{ \left(0.35 \times \left(1 - \frac{160}{148.4}\right)^2\right) + \left(0.2 \times \left(1 - \frac{151}{148.4}\right)^2\right) + \left(0.35 \times \left(1 - \frac{143}{148.4}\right)^2\right) \right. $$
$$\left. + \left(0.05 \times \left(1 - \frac{146}{148.4}\right)^2\right) + \left(0.05 \times \left(1 - \frac{142}{148.4}\right)^2\right) \right\}^{0.5} = 5.263\%$$

Thus, both the parameters Ω and δ are important for predicting the solid-solution formation rule: more Ω and less δ would facilitate solid-solution formation. For this selected composition of alloy, the δ value is within the limit ($0 \leq \delta \leq 6.5$) defined for the formation of solid solution in HEA. Therefore, the selected multi-component alloy $Al_{35}Li_{20}Mg_{35}Ti_5Zn_5$ is a suitable candidate for the synthesis of LWHEA as per the theoretical calculation and HEA design criterion.

3. Processing of LWHEAs

A variety of processing routes has been used for the synthesis of HEAs such as melting and casting route, powder metallurgy route, and deposition techniques. Melting and casting techniques, with equilibrium and nonequilibrium cooling rates, have been used to produce HEAs in the shape of rods, bars, and ribbons. The most popular melt processing techniques are vacuum arc melting, vacuum induction melting, and melt spinning. Mechanical alloying (MA) followed by sintering has been the major solid-state processing route to produce sintered products. Sputtering, plasma nitriding, and cladding are the surface modification techniques used to produce thin films and thick layers of HEAs on various substrates. For LWHEA, an addition of low-density metals (Mg, Al, Ti, Be, Sc, and Li) is the criterion for designing, therefore, vacuum arc melting and mechanical alloying followed by sintering are the two main processing techniques that have been used by researchers [22–29].

3.1. Melting and Casting Route

Almost 3/4th of the total research on HEAs that has been reported so far used vacuum arc melting as processing technique and few used vacuum induction melting process. The reason for using vacuum arc melting is due to high temperature (up to 3000 °C) that can be realized, which is sufficient to melt most of the metals used for LWHEAs. However, this technique is not suitable for an alloy having certain low-boiling point elements due to the possibility of evaporation during melting, which makes compositional control more difficult. In such cases, induction and resistance heating furnaces have been adopted for making the alloys. The alloys of CrNbTiVZr and Al_xNbTiVZr systems were cast using the arc melting technique, as most of the elements of alloys melt at high temperature [23,25]. One main constraint in the melting and casting route is the development of heterogeneous microstructure due to segregation caused by the slow rate of solidification. Therefore, homogenization treatment has to be performed to reduce the effect of heterogeneity in the microstructure. Some other alloys including $Al_{20}Be_{20}Fe_{10}Si_{15}Ti_{35}$ and $Mg_x(AlCuMnZn)_{100-x}$ were also synthesized using induction melting and casting route [26,27].

3.2. Mechanical Alloying and Consolidation

A small fraction of about 5% of the reports on HEAs so far deals with the synthesis of HEAs by solid-state processing, which involves Mechanical Alloying (MA) of the elemental blends followed by consolidation. For the production of real LWHEA (<3 g·cm^{-3} density), MA is an important processing route. Most of the elements added to reduce the density may exhibit large variation in melting temperature, such as in AlFeMgTiZn alloy [72], Mg having 650 °C and Ti having 1668 °C as their melting temperatures. MA is the process of high-energy ball milling of elemental powder blends, which involves diffusion of species into each other in order to obtain a homogeneous alloy. This technique was first developed by Benjamin et al. for the synthesis of oxide dispersion strengthened Ni-base superalloys [73]. High-energy ball milling involves continuous deformation, fracture, and welding of particles, which finally leads to the nanocrystallization or even amorphization. Vincent et al. [72] produced AlFeMgTiZn LWHEA using the high energy MA and studied the effect of milling time on the structure of the alloy. In another work to synthesize $Al_{20}Li_{20}Mg_{10}Sc_{20}Ti_{30}$ alloy, Youssef et al. [30] used high energy MA as the processing route.

After powder compaction in MA technique, the green compact needs to be sintered to achieve high density. In LWHEA, there are many elements that exhibit a large difference in melting temperature and their quantity is also very significant (at least >5%). Therefore, use of conventional sintering method of nanocrystalline alloy powders will lead to complete melting of one of the elements in the alloy, while other elements will be in solid state.

In order to overcome this problem, another method is used for quick sintering of nanocrystalline alloys obtained by MA, spark plasma sintering (SPS). SPS involves the application of high amperage pulsed current (up to 5000 A) through the sample kept usually in a graphite die, while simultaneously applying pressures to the tune of about 100 MPa, as shown in Figure 1. The pulsed current leads to the formation of spark plasma at the particle-particle interface in short periods causing almost instantaneous heating of the powder particles. This leads to sintering being completed within a few minutes in contrast to conventional sintering which takes a few hours.
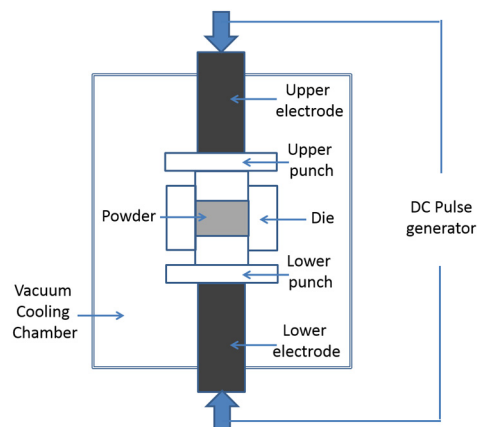

Figure 1. Schematic diagram of mechanical alloying using spark plasma sintering method.

Table 2 summarizes the various processing techniques used to synthesize different HEAs from high density to LWHEA. Three HEAs, NbTiVTa, HfNbTaTiZr and $Hf_{27.5}Nb_5Ta_5Ti_{35}Zr_{27.5}$ [19–21], are only considered to show a trend in the evolution of LWHEA. Actual development of LWHEA is started from NbTiVZr alloy onwards [24]. Either casting or MA method of processing is used to fabricate the LWHEA in the reported alloys. From the reported values, it is clear that for obtaining comparatively high-density HEA, melting and casting method of processing is preferable. This is because that high-density element, such as Nb, V, Zr and Fe, exhibits higher melting point. For comparatively lower density HEA (below 3 g·cm^{-3}), lighter elements such as Al, Mg, Be, Li, Sc

and Ti have been used. Most of these elements have low melting point and there are higher chances of evaporation by melting and casting route; therefore, MA is used as the preferred processing method. Using MA and sintering processes, Youssef et al. [30] fabricated single phase FCC HEA which is the only single phase reported low-density HEA.

Table 2. List of HEAs from high density to low density (LWHEA), their processing routes and various solid solution phases observed in microstructure.

Alloy	Density (g/cc)	Process	Phase	Source
NbTiVTa	11.49	Arc melting	BCC	[19]
HfNbTaTiZr	9.94	Arc melting	BCC	[20]
$Hf_{27.5}Nb_5Ta_5Ti_{35}Zr_{27.5}$	8.48	Arc melting	orthorhombic	[21]
NbTiVZr	6.49		BCC	
$Al_{0.5}NbTiVZr$	6.04	Arc melting	BCC	[25]
AlNbTiVZr	5.79		BCC	
$Al_{1.5}NbTiVZr$	5.55		BCC	
$Al_{26.6}Nb_{23.8}Ti_{25.1}V_{24.5}$	5.59	Casting	BCC	[74]
$Al_{20}Be_{20}Fe_{10}Si_{15}Ti_{35}$	3.91	Casting	3 phases	[26]
$Mg_{20}(AlCuMnZn)_{80}$	4.29			
$Mg_{33}(AlCuMnZn)_{67}$	3.26		HCP+ Al-Mn	
$Mg_{43}(AlCuMnZn)_{57}$	2.51	Induction melting	icosahedral	[27]
$Mg_{45.6}(AlCuMnZn)_{54.4}$	2.30		Quasi-crystal	
$Mg_{50}(AlCuMnZn)_{50}$	2.20			
$Al_{20}Li_{20}Mg_{10}Sc_{20}Ti_{30}$	2.67	MA	FCC	[30]

4. Microstructural Characteristics of LWHEA

Table 2 shows the different phases found in the different HEAs from high density to LWHEA. Stepanov et al. [25] studied the effect of Al addition to the NbTiVZr alloy and found that the base alloy has BCC structure with tiny amount of Laves (C14) phase (Laves phase is intermetallic compounds that have a stoichiometry of AB_2). The addition of Al stabilizes the Laves phase due to the formation of Zr_2Al and reduces the amount of BCC phase. While another alloy, $Al_{26.6}Nb_{23.8}Ti_{25.1}V_{24.5}$ synthesized by Stepanov et al. [74] containing a high amount of Al shows single phase BCC structure in dendritic form. The theoretical criterion for the solid solution structure also predicts the BCC structure for this alloy as VEC = 4.24 (<6.87). Li et al. [27] synthesized HEA using Mg with equiatomic AlCuMnZn alloy in different atomic percentage from 20 to 50. It was found that microstructure contains Al-Mn icosahedral phase which was a thermally-stable phase and a HCP phase in $Mg_{20}(AlCuMnZn)_{80}$ alloy. As the Mg concentration increased, the number of phases also increased to four including Mg and Mg_7Zn_3 phases. Youssef et al. formed $Al_{20}Li_{20}Mg_{10}Sc_{20}Ti_{30}$ HEA using MA route rather the melting and casting route. Two similar compositions were prepared, but one is without the contamination of N, O impurity and other contaminated with N, O impurity. Alloy without impurity resulted in a single phase FCC crystal structure, which later converted to HCP after annealing at 500 °C. Alloy with impurity also showed the single phase FCC crystal structure but it remained FCC even after annealing at 500 °C. As the MA techniques for fabrication is subjected to the formation of alloy in solid state conditions, they are not thermodynamically stable. Therefore, some changes in the microstructure are expected if any heat treatment performed on the material due to bring thermal stability in the material.

5. Mechanical Properties of LWHEA

Most of the lightweight alloys were tested for their mechanical properties. It was found that in most of the studies there are only two tests performed for mechanical characterization, hardness and compressive properties. This section contains the result of hardness and compression test for the different LWHEA.

Table 3 shows a trend of microhardness values for different HEAs. Results for AlNbTiVZr alloy shows that hardness value increases by the addition of Al in NbTiVZr alloy from 380 Hv to 620 Hv.

This was attributed to the formation of the Laves phase. As the Al concentration increased, the amount of Laves phase was found to be increasing. Homogenization treatment changed the hardness value of NbTiVZr alloy but no significant effect was observed in Al-containing samples. Another alloy, $Al_{26.6}Nb_{23.8}Ti_{25.1}V_{24.5}$, contains a high amount of Al, therefore, the hardness value observed is 448 Hv only [74].

Table 3. Trend of microhardness in different HEAs.

Alloy	Density (g/cc)	Micro-Hardness (Hv)	
		As Solidified	**Homogenised**
NbTiVTa	11.49	NA	
HfNbTaTiZr	9.94	390 ± 8	
$Hf_{27.5}Nb_5Ta_5Ti_{35}Zr_{27.5}$	8.48	245	
NbTiVZr	6.49	380 ± 10	460 ± 10
$Al_{0.5}NbTiVZr$	6.04	470 ± 10	500 ± 20
AlNbTiVZr	5.79	540 ± 10	550 ± 20
$Al_{1.5}NbTiVZr$	5.55	620 ± 20	630 ± 30
$Al_{26.6}Nb_{23.8}Ti_{25.1}V_{24.5}$	5.59	448 ± 12	
$Al_{20}Be_{20}Fe_{10}Si_{15}Ti_{35}$	3.91	911	
$Mg_{20}(AlCuMnZn)_{80}$	4.29	429	
$Mg_{33}(AlCuMnZn)_{67}$	3.26	315	
$Mg_{43}(AlCuMnZn)_{57}$	2.51	255	
$Mg_{45.6}(AlCuMnZn)_{54.4}$	2.30	225	
$Mg_{50}(AlCuMnZn)_{50}$	2.20	178	
$Al_{20}Li_{20}Mg_{10}Sc_{20}Ti_{30}$	2.67	591.4 (as milled)	499.6 (annealed at 500 °C)

This is due to less solution strengthening effect, as only four different elements are present compared to five elements alloy. $Al_{20}Be_{20}Fe_{10}Si_{15}Ti_{35}$ alloy shows extremely high hardness value (911 Hv) compared to other lightweight HEAs [26]. Mg-based LWHEAs designed by Li et al. [27] revealed that addition of Mg lowers the hardness value from 429 Hv to 178 Hv. This was attributed to the decrease in solution strengthening for a higher concentration of Mg. $Al_{20}Li_{20}Mg_{10}Sc_{20}Ti_{30}$ alloy shows higher hardness value compared to $Mg_x(AlCuMnZn)_{100-x}$ alloys, even the density value is significantly less from many of the compositions.

Table 4 contains the compression stress-strain results for most of the reported LWHEAs. AlNbTiVZr alloy shows that addition of 0.5% Al initially lowers the yield stress then a slight increase for 1% Al and for 1.5% Al yield point is not observed. Fracture strain also decreased by the addition of Al from 4.2% to 0%, as for $Al_{1.5}NbTiVZr$ there is no plastic deformation and the specimen fractured at 1310 MPa. Fractography results revealed that multiple cracks developed, which were aligned or at 45° from the compression direction. $Mg_x(AlCuMnZn)_{100-x}$ alloys exhibit high compressive strength but the fracture strain was poor. Solution strengthening and quasicrystal dispersion strengthening are the two main mechanisms for strengthening of these alloys. High confusion atoms in the lattice and the atomic radius difference increased the lattice distortion energy to a high. Dislocations in the alloys are hard to move and that is why the strength was found to be high. As the microstructure contains HCP phase, therefore, fewer slip systems are available and this is the reason for low plasticity. Slight increase in plastic strain for 50% Mg-containing alloy was attributed to the decrease in solution strengthening.

Table 4. List of compression yield stress, peak stress and fracture strain values for different HEAs.

Alloy	Density (g/cc)	Yield Stress (MPa)	Peak Stress (MPa)	Fracture Strain (%)
NbTiVTa	11.49	1092	NA	>50
HfNbTaTiZr	9.94	929	NA	>50
$Hf_{27.5}Nb_5Ta_5Ti_{35}Zr_{27.5}$	8.48	NA	NA	NA
NbTiVZr	6.49	1320	1470	4.2
$Al_{0.5}NbTiVZr$	6.04	960	1100	4
AlNbTiVZr	5.79	1080	1210	2.3
$Al_{1.5}NbTiVZr$	5.55	NA	1310	0
$Al_{26.6}Nb_{23.8}Ti_{25.1}V_{24.5}$	5.59	1020	1318	5
$Mg_{20}(AlCuMnZn)_{80}$	4.29	428	428	3.29
$Mg_{33}(AlCuMnZn)_{67}$	3.26	437	437	3.41
$Mg_{43}(AlCuMnZn)_{57}$	2.51	500	500	3.72
$Mg_{45.6}(AlCuMnZn)_{54.4}$	2.30	482	482	4.06
$Mg_{50}(AlCuMnZn)_{50}$	2.20	340	400	4.83

6. Future Directions for the Development LWHEAs

Despite the many existing processing techniques, there are still many challenges in the processing of HEAs. One major issue is the segregation problem in melting and casting route. In the perspective of these challenges, some new material synthesis techniques are being discussed as a part of possible future synthesis techniques for LWHEAs. We believe that if the suggested processing techniques are utilized to synthesize LWHEA, even better properties and overall low density can be achieved. These techniques include the synthesis of porous LWHEA structures, microwave sintering of green compact, casting of LWHEA using disintegration melt deposition (DMD) technique and fabrication of component using direct additive manufacturing using HEA powder.

6.1. Synthesis of Porous Structured LWHEA

Porous structures are good for structural as well for biomedical applications. For structural applications, high strength to weight ratio can be achieved using porous structures. For biomedical applications, porous structures allow adequate space for transportation of nutrients and for the growth of living tissues [75]. By adjusting the porosity, modulus can be controlled in the porous structure. This provides an opportunity to design materials with the properties more closely to that of natural bone and the issue of stress shielding can be addressed properly [76]. Fabrication of LWHEA with interconnected pores is possible by mixing space holder particles with HEA powder followed by compaction of powder. The particles can later be leached out by dissolving the material in a suitable solution or evaporated by thermal decomposition during sintering. The critical step of this process is the selection of space holder particles, especially when materials are designed for biomedical applications. These particles should completely evaporate or leach out from the material without any contamination [77]. Commonly used space holder particles are sodium chloride, ammonium bicarbonate and carbamide ($CO(NH_2)_2$) [78–80]. Selection of quantity and size of the space holder particles depend on the size and porosity level requirements of HEA material.

Recently, Čapek et al. [79] synthesized porous magnesium structures using ammonium bicarbonate as space holder particles. Mg powder (75–150 μm) and ammonium bicarbonate powder (250–500 μm) were used to synthesize Mg-containing 0, 5, 10, 15, and 20 vol % ammonium bicarbonate materials. These powders were mixed manually for 30 min with 30 vol % liquid hexane to avoid segregation followed by the compaction into a cylindrical die at a pressure of 265 MPa. The green compacts were then heat-treated at 130 °C for 4 h using a muffle furnace followed by sintering at 550 °C for 6 h using a tubular furnace. Ammonium bicarbonate gets decomposed at 130 °C and created porosity in the compacts. After sintering of different volume percent of ammonium bicarbonate samples, 12, 23, 28, 33, and 38 vol %, porosity was recorded. These samples were then characterized by microstructure, flexural strength, and corrosion properties under physiological conditions. Magnesium

with least porosity (12 vol %) exhibited the best flexural strength and corrosion properties. A similar approach can be used to develop porous LWHEA materials. This synthesis technique is also useful to fabricate porous structures from high-density HEA alloys, which exhibit good structural properties. Because of porosity, the density of HEA will be significantly reduced for lightweight application. Some decrease in the structural properties would also occur, but overall the properties of porous HEA will be much better than the existing lightweight materials. This concept of fabrication of porous HEAs is relatively new and it has not been investigated yet.

6.2. Use of Powder Metallurgy with Microwave Sintering Route

Another proposed method to synthesize LWHEA in solid state is the use of powder metallurgy technique incorporating microwave sintering. In conventional powder metallurgy, once powder is blended, cold press or hot press or hot isostatic press is used to produce a "green compact", which is approximately 80% dense. The sintering process creates bonding between the powders and minimizes the porosity. Conventional sintering is done by using a traditional resistance heating furnace [81,82], in which green compact is heated from outer surface to inner core of the powder compact. This results in poor microstructural properties in the core of the material [83]. Microwaves can be utilized to sinter the green compact as it utilizes both electric and magnetic field to sinter the compact. This technique results in higher densities or less porosity compared to the conventional sintering at the cheaper cost [84]. There are two important advantages to using microwave sintering [84]: shorter sintering time and lower sintering temperatures. In hybrid microwave sintering, two crucibles are used, one inside the other with a layer of silicon carbide (SiC) susceptor in between. The SiC layer absorbs microwave energy readily and is thereby heated up quickly. The green compact is placed in the inner crucible and heated up by both the microwaves and SiC susceptor. To the best of the authors' knowledge, no work has been done to synthesize LWHEAs using MA-assisted microwave sintering process with two-directional heating. If this technique were used for the synthesis of LWHEA, better mechanical properties could be realized, as reported in the literature for other Mg-based materials [83].

6.3. Synthesis of LWHEA Using Disintegration Meld Deposition Technique

Another unique synthesis technique that can be used for the synthesis of LWHEAs is disintegration melt deposition (DMD) technique. Figure 2 shows a schematic diagram of DMD technique, which was developed in early 1990s [85]. DMD is a processing technique, which brings together the cost-effectiveness associated with conventional casting process and scientific innovativeness and technological potential associated with spray forming process. However, unlike spray forming, DMD technique uses lower impinging gas jet velocity. Within a graphite crucible, the alloy material is superheated above the melting temperature under the Ar gas atmosphere using a resistance heating furnace. For achieving homogeneous composition, the superheated slurry is stirred at 465 rpm for 5–10 min using a twin blade with a pitch of $45°$.

After stirring, the molten metal is then allowed to downpour into the mold, under the influence of gravity, through a 10-mm hole in the crucible. Before entering the mold, the molten metal is disintegrated by two jets of Ar gas oriented normal to the melt stream. The flow rate of Ar is maintained at 25 L/min, and an ingot of desirable size is normally obtained. DMD is one of the most effective solidification routes to synthesize aluminium and magnesium based alloys [86,87], bulk metallic glass [88], and composites with reinforcements at micron, submicron, and nano-scales [89–95]. Mg and Al are two lightweight components in order to design a LWHEA for structural applications. DMD has already been reported for synthesizing good quality Mg and Al-based alloy due to their fine grain structure. Therefore, use of DMD for synthesizing LWHEAs would result in even better structural properties compared to the existing methods used for the same.
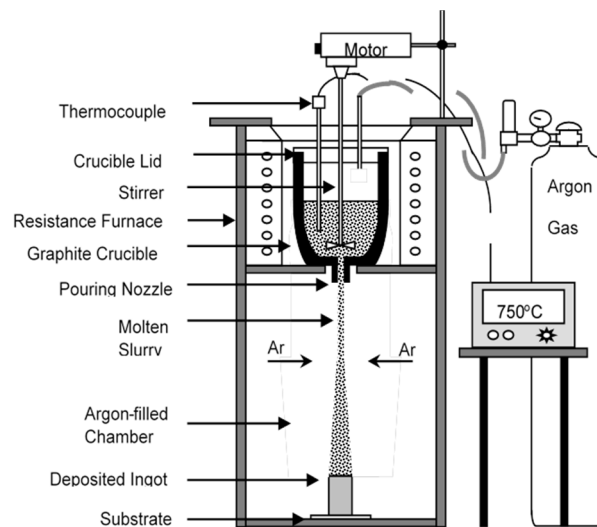
Figure 2. Schematic diagram of disintegrated melt deposition technique [95].

6.4. Use of Additive Manufacturing Technique

Additive manufacturing is a recently developed technique, which is also known as rapid manufacturing or rapid prototyping. It is used to create metal and polymer parts layer by layer and is competent to fabricate highly complex shape objects. An object model is first designed in CAD software, and then the software slices the designed part into many layers with every layer defined by a layer thickness, and the object is fabricated in a layer-by-layer fashion [96].

Selective laser melting (SLM) is the process commonly used to selectively melt the powder by using the energy of a laser beam. A bottom-to-top approach is usually utilized such that once the first layer of available powder is sintered, a new layer of powder is deposited, which is subsequently sintered. No support structures are utilized to build simple structures but, for more complicated structures, building support structures is required. SLM method is currently used to synthesize the components made of polymers, ceramic powders, and metallic powders. The microstructure and mechanical properties of SLM sintered parts largely depend on the laser power and laser scan speed utilized during synthesis [97]. This technique is suitable for direct manufacturing of components using HEA powder after mechanical alloying. Figure 3 shows a schematic diagram of additive manufacturing or rapid prototyping.
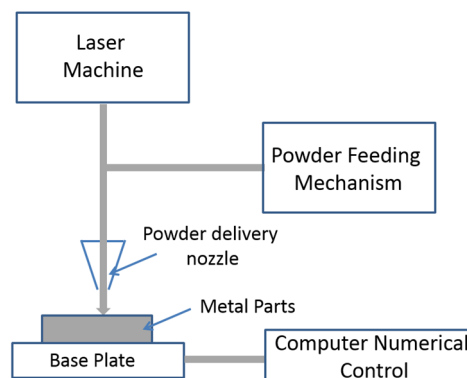

Figure 3. Schematic diagram of rapid prototyping technique.

7. Research Lapses

In this review, an insight into the evolution of LWHEAs is provided, and many new synthesis methods have been proposed that can created a breakthrough in this direction. Extensive research efforts are being made to develop HEAs for many structural applications because of its excellent strength, antioxidation and anticorrosion properties. Still, HEAs have not been explored for many applications. Although many HEAs have been designed and studied recently, their tensile test performance has rarely been explored. Instead, mechanical properties are often characterized in terms of compression tests or hardness. Most of the LWHEAs designed to date have very limited tensile ductility, often not exceeding a few percent of strain prior to fracture. Density is one of the main constraints for the future application of HEA in lightweight applications such as in transportation, energy and biomedical sectors. High entropy alloy systems developed so far with a density of <3 g·cm^{-3} are extremely limited. Much more research efforts are required in this area. Because of their high strength and anticorrosion properties, HEAs are potential candidates for biomedical applications. The porous structure is one of the examples for the application of LWHEA in the biomedical area. For structural applications, DMD can be an effective technique to achieve homogenous microstructure and a good combination of mechanical properties. Microwave sintering is one of the most cost-effective methods of sintering for powder metallurgy routes. This technique should be investigated to study the difference in the properties of LWHEA in comparison to other sintering techniques. Additive manufacturing is another fast growing technique for manufacturing complex shapes without any support structure. As the technique is based on powder processing, LWHEA powder after manufacturing can be directly converted to the final component. The possibility of manufacturing porous components using LWHEA powder by additive manufacturing should also be explored.

Conflicts of Interest: The authors declare no conflict of interest.

References

1. Schubert, E.; Klassen, M.; Zerner, I.; Walz, C.; Sepold, G. Light-weight structures produced by laser beam joining for future applications in automobile and aerospace industry. *J. Mater. Process. Technol.* **2001**, *115*, 2–8. [CrossRef]

2. Cheah, L.W. Cars on a diet: The Material and Energy Impacts of Passenger Vehicle Weight Reduction in the US. Ph.D. Thesis, Massachusetts Institute of Technology, Cambridge, MA, USA, 2010.

3. Miller, W.; Zhuang, L.; Bottema, J.; Wittebrood, A.J.; De Smet, P.; Haszler, A.; Vieregge, A. Recent development in aluminium alloys for the automotive industry. *Mater. Sci. Eng. A* **2000**, *280*, 37–49. [CrossRef]

4. Yeh, J.W.; Chen, S.K.; Lin, S.J.; Gan, J.Y.; Chin, T.S.; Shun, T.T.; Tsau, C.H.; Chang, S.Y. Nanostructured High-Entropy Alloys with Multiple Principal Elements: Novel Alloy Design Concepts and Outcomes. *Adv. Eng. Mater.* **2004**, *6*, 299–303. [CrossRef]

5. Yeh, J.-W.; Lin, S.-J.; Chin, T.-S.; Gan, J.-Y.; Chen, S.-K.; Shun, T.-T.; Tsau, C.-H.; Chou, S.-Y. Formation of simple crystal structures in Cu-Co-Ni-Cr-Al-Fe-Ti-V alloys with multiprincipal metallic elements. *Metall. Mater. Trans. A* **2004**, *35*, 2533–2536. [CrossRef]

6. Tong, C.-J.; Chen, Y.-L.; Yeh, J.-W.; Lin, S.-J.; Chen, S.-K.; Shun, T.-T.; Tsau, C.-H.; Chang, S.-Y. Microstructure characterization of Al$_x$CoCrCuFeNi high-entropy alloy system with multiprincipal elements. *Metall. Mater. Trans. A* **2005**, *36*, 881–893. [CrossRef]

7. Chen, T.-K.; Shun, T.; Yeh, J.; Wong, M. Nanostructured nitride films of multi-element high-entropy alloys by reactive DC sputtering. *Surf. Coat. Technol.* **2004**, *188*, 193–200. [CrossRef]

8. Tong, C.-J.; Chen, M.-R.; Yeh, J.-W.; Lin, S.-J.; Chen, S.-K.; Shun, T.-T.; Chang, S.-Y. Mechanical performance of the Al$_x$CoCrCuFeNi high-entropy alloy system with multiprincipal elements. *Metall. Mater.Trans. A* **2005**, *36*, 1263–1271. [CrossRef]

9. Huang, P.K.; Yeh, J.W.; Shun, T.T.; Chen, S.K. Multi-Principal-Element Alloys with Improved Oxidation and Wear Resistance for Thermal Spray Coating. *Adv. Eng. Mater.* **2004**, *6*, 74–78. [CrossRef]

10. Chen, Y.; Duval, T.; Hung, U.; Yeh, J.; Shih, H. Microstructure and electrochemical properties of high entropy alloys—A comparison with type-304 stainless steel. *Corros. Sci.* **2005**, *47*, 2257–2279. [CrossRef]

11. Chen, Y.; Hong, U.; Shih, H.; Yeh, J.; Duval, T. Electrochemical kinetics of the high entropy alloys in aqueous environments—A comparison with type 304 stainless steel. *Corros. Sci.* **2005**, *47*, 2679–2699. [CrossRef]

12. Hsu, C.-Y.; Yeh, J.-W.; Chen, S.-K.; Shun, T.-T. Wear resistance and high-temperature compression strength of Fcc CuCoNiCrAl$_{0.5}$Fe alloy with boron addition. *Metall. Mater. Trans. A* **2004**, *35*, 1465–1469. [CrossRef]

13. Gao, M.C.; Yeh, J.-W.; Liaw, P.K.; Zhang, Y. *High-Entropy Alloys: Fundamentals and Applications*; Springer: Cham, Switzerland, 2016.

14. Industrial Development of High-Entropy Alloys. Masson. Available online: https://www.scribd.com/document/269966894/The-Industrial-Development-of-High-Entropy-Alloys (accessed on 24 August 2016).

15. Gludovatz, B.; Hohenwarter, A.; Catoor, D.; Chang, E.H.; George, E.P.; Ritchie, R.O. A fracture-resistant high-entropy alloy for cryogenic applications. *Science* **2014**, *345*, 1153–1158. [CrossRef] [PubMed]

16. Glicksman, M.E. *Principles of Solidification: An Introduction to Modern Casting and Crystal Growth Concepts*; Springer Science & Business Media: New York, NY, USA, 2010.

17. Zhang, Y.; Zuo, T.T.; Tang, Z.; Gao, M.C.; Dahmen, K.A.; Liaw, P.K.; Lu, Z.P. Microstructures and properties of high-entropy alloys. *Prog. Mater. Sci.* **2014**, *61*, 1–93. [CrossRef]

18. Huang, Y.-S. Recent Patents on High-Entropy Alloy. *Recent Pat. Mater. Sci.* **2009**, *2*, 154–157. [CrossRef]

19. Frazier, W.E.; Lee, E.W.; Donnellan, M.E.; Thompson, J.J. Advanced lightweight alloys for aerospace applications. *JOM* **1989**, *41*, 22–26. [CrossRef]

20. Yang, X.; Zhang, Y.; Liaw, P. Microstructure and compressive properties of NbTiVTaAl$_x$ high entropy alloys. *Proced. Eng.* **2012**, *36*, 292–298. [CrossRef]

21. Senkov, O.; Scott, J.; Senkova, S.; Miracle, D.; Woodward, C. Microstructure and room temperature properties of a high-entropy TaNbHfZrTi alloy. *J. Alloy. Compd.* **2011**, *509*, 6043–6048. [CrossRef]

22. Lilensten, L.; Couzinié, J.; Perrière, L.; Bourgon, J.; Emery, N.; Guillot, I. New structure in refractory high-entropy alloys. *Mater. Lett.* **2014**, *132*, 123–125. [CrossRef]

23. Senkov, O.; Senkova, S.; Woodward, C.; Miracle, D. Low-density, refractory multi-principal element alloys of the Cr-Nb-Ti-V-Zr system: Microstructure and phase analysis. *Acta Mater.* **2013**, *61*, 1545–1557. [CrossRef]

24. Senkov, O.; Senkova, S.; Miracle, D.; Woodward, C. Mechanical properties of low-density, refractory multi-principal element alloys of the Cr-Nb-Ti-V-Zr system. *Mater. Sci. Eng. A* **2013**, *565*, 51–62. [CrossRef]

25. Stepanov, N.; Yurchenko, N.Y.; Shaysultanov, D.; Salishchev, G.; Tikhonovsky, M. Effect of Al on structure and mechanical properties of Al$_x$NbTiVZr (x = 0, 0.5, 1, 1.5) high entropy alloys. *Mater. Sci. Technol.* **2015**, *31*, 1184–1193. [CrossRef]

26. A Novel Light High-Entropy Alloy Al$_{20}$Be$_{20}$Fe$_{10}$Si$_{15}$Ti$_{35}$. Available online: http://www.science24.com/paper/19071 (accessed on 25 August 2016).

27. Li, R.; Gao, J.C.; Fan, K. Study to microstructure and mechanical properties of Mg containing high entropy alloys. *Mater. Sci. Forum* **2010**, *650*, 265–271. [CrossRef]

28. Li, R.; Gao, J.C.; Fan, K. Microstructure and mechanical properties of MgMnAlZnCu high entropy alloy cooling in three conditions. *Mater. Sci. Forum* **2011**, *686*, 235–241. [CrossRef]

29. Chen, Y.-L.; Tsai, C.-W.; Juan, C.-C.; Chuang, M.-H.; Yeh, J.-W.; Chin, T.-S.; Chen, S.-K. Amorphization of equimolar alloys with HCP elements during mechanical alloying. *J. Alloy. Compd.* **2010**, *506*, 210–215. [CrossRef]

30. Youssef, K.M.; Zaddach, A.J.; Niu, C.; Irving, D.L.; Koch, C.C. A novel low-density, high-hardness, high-entropy alloy with close-packed single-phase nanocrystalline structures. *Mater. Res. Lett.* **2015**, *3*, 95–99. [CrossRef]

31. Gaskell, D.R. *Introduction to the Thermodynamics of Materials*; CRC Press: Boca Raton, LA, USA, 2008.

32. Jien-Wei, Y. Recent progress in high entropy alloys. *Ann. Chim. Sci. Mat.* **2006**, *31*, 633–648.

33. Yeh, J.-W. Alloy design strategies and future trends in high-entropy alloys. *JOM* **2013**, *65*, 1759–1771. [CrossRef]

34. Tsai, K.-Y.; Tsai, M.-H.; Yeh, J.-W. Sluggish diffusion in Co-Cr-Fe-Mn-Ni high-entropy alloys. *Acta Mater.* **2013**, *61*, 4887–4897. [CrossRef]

35. Takeuchi, A.; Amiya, K.; Wada, T.; Yubuta, K.; Zhang, W.; Makino, A. Entropies in alloy design for high-entropy and bulk glassy alloys. *Entropy* **2013**, *15*, 3810–3821. [CrossRef]

36. Zhang, Y.; Zhou, Y.J.; Lin, J.P.; Chen, G.L.; Liaw, P.K. Solid-solution phase formation rules for multi-component alloys. *Adv. Eng. Mater.* **2008**, *10*, 534–538. [CrossRef]

37. Zhang, Y.; Yang, X.; Liaw, P. Alloy design and properties optimization of high-entropy alloys. *JOM* **2012**, *64*, 830–838. [CrossRef]

38. Yang, X.; Zhang, Y. Prediction of high-entropy stabilized solid-solution in multi-component alloys. *Mater. Chem. Phys.* **2012**, *132*, 233–238. [CrossRef]

39. Sheng, G.; Liu, C.T. Phase stability in high entropy alloys: formation of solid-solution phase or amorphous phase. *Prog. Nat. Sci. Mater. Int.* **2011**, *21*, 433–446.

40. Varalakshmi, S.; Kamaraj, M.; Murty, B. Processing and properties of nanocrystalline CuNiCoZnAlTi high entropy alloys by mechanical alloying. *Mater.Sci. Eng. A* **2010**, *527*, 1027–1030. [CrossRef]

41. Senkov, O.; Wilks, G.; Scott, J.; Miracle, D. Mechanical properties of $Nb_{25}Mo_{25}Ta_{25}W_{25}$ and $V_{20}Nb_{20}Mo_{20}Ta_{20}W_{20}$ refractory high entropy alloys. *Intermetallics* **2011**, *19*, 698–706. [CrossRef]

42. Cantor, B.; Chang, I.; Knight, P.; Vincent, A. Microstructural development in equiatomic multicomponent alloys. *Mater. Sci. Eng. A* **2004**, *375*, 213–218. [CrossRef]

43. Pradeep, K.; Wanderka, N.; Choi, P.; Banhart, J.; Murty, B.; Raabe, D. Atomic-scale compositional characterization of a nanocrystalline AlCrCuFeNiZn high-entropy alloy using atom probe tomography. *Acta Mater.* **2013**, *61*, 4696–4706. [CrossRef]

44. Otto, F.; Yang, Y.; Bei, H.; George, E.P. Relative effects of enthalpy and entropy on the phase stability of equiatomic high-entropy alloys. *Acta Mater.* **2013**, *61*, 2628–2638. [CrossRef]

45. Singh, S.; Wanderka, N.; Murty, B.; Glatzel, U.; Banhart, J. Decomposition in multi-component AlCoCrCuFeNi high-entropy alloy. *Acta Mater.* **2011**, *59*, 182–190. [CrossRef]

46. Shun, T.-T.; Chang, L.-Y.; Shiu, M.-H. Microstructure and mechanical properties of multiprincipal component $CoCrFeNiMo_x$ alloys. *Mater. Charact.* **2012**, *70*, 63–67. [CrossRef]

47. Singh, S.; Wanderka, N.; Kiefer, K.; Siemensmeyer, K.; Banhart, J. Effect of decomposition of the Cr-Fe-Co rich phase of AlCoCrCuFeNi high entropy alloy on magnetic properties. *Ultramicroscopy* **2011**, *111*, 619–622. [CrossRef] [PubMed]

48. Deng, Y.; Tasan, C.C.; Pradeep, K.G.; Springer, H.; Kostka, A.; Raabe, D. Design of a twinning-induced plasticity high entropy alloy. *Acta Mater.* **2015**, *94*, 124–133. [CrossRef]

49. Tasan, C.C.; Deng, Y.; Pradeep, K.G.; Yao, M.; Springer, H.; Raabe, D. Composition dependence of phase stability, deformation mechanisms, and mechanical properties of the CoCrFeMnNi high-entropy alloy system. *JOM* **2014**, *66*, 1993–2001. [CrossRef]

50. Yao, M.; Pradeep, K.; Tasan, C.; Raabe, D. A novel, single phase, non-equiatomic FeMnNiCoCr high-entropy alloy with exceptional phase stability and tensile ductility. *Scr. Mater.* **2014**, *72*, 5–8. [CrossRef]

51. Raabe, D.; Tasan, C.C.; Springer, H.; Bausch, M. From High-Entropy Alloys to High-Entropy Steels. *Steel Res. Int.* **2015**, *86*, 1127–1138. [CrossRef]

52. Ye, Y.; Wang, Q.; Lu, J.; Liu, C.; Yang, Y. Design of high entropy alloys: A single-parameter thermodynamic rule. *Scr. Mater.* **2015**, *104*, 53–55. [CrossRef]

53. Ye, Y.; Wang, Q.; Lu, J.; Liu, C.; Yang, Y. The generalized thermodynamic rule for phase selection in multicomponent alloys. *Intermetallics* **2015**, *59*, 75–80. [CrossRef]

54. Guo, S.; Ng, C.; Lu, J.; Liu, C. Effect of valence electron concentration on stability of fcc or bcc phase in high entropy alloys. *J. Appl. Phys.* **2011**, *109*, 103505. [CrossRef]

55. Kohn, W.; Sham, L.J. Self-consistent equations including exchange and correlation effects. *Phys. Rev.* **1965**, *140*, A1133. [CrossRef]

56. Gao, M.C.; Alman, D.E. Searching for next single-phase high-entropy alloy compositions. *Entropy* **2013**, *15*, 4504–4519. [CrossRef]

57. Senkov, O.; Miller, J.; Miracle, D.; Woodward, C. Accelerated exploration of multi-principal element alloys with solid solution phases. *Nat. Commun.* **2015**, *6*, 6529. [CrossRef] [PubMed]

58. Zhang, C.; Zhang, F.; Chen, S.; Cao, W. Computational thermodynamics aided high-entropy alloy design. *JOM* **2012**, *64*, 839–845. [CrossRef]

59. Miracle, D.B.; Miller, J.D.; Senkov, O.N.; Woodward, C.; Uchic, M.D.; Tiley, J. Exploration and development of high entropy alloys for structural applications. *Entropy* **2014**, *16*, 494–525. [CrossRef]

60. Zhang, C.; Gao, M.C. *CALPHAD Modeling of High-Entropy Alloys, in High-Entropy Alloys*; Springer: Cham, Switzerland, 2016; pp. 399–444.

61. Ye, Y.; Wang, Q.; Lu, J.; Liu, C.; Yang, Y. High-entropy alloy: challenges and prospects. *Mater. Today* **2015**, *19*, 349–362. [CrossRef]

62. Gao, M.; Zhang, B.; Guo, S.; Qiao, J.; Hawk, J. High-entropy alloys in hexagonal close-packed structure. *Metall. Mater. Trans. A* **2016**, *47*, 3322–3332. [CrossRef]

63. Li, C.; Li, J.; Zhao, M.; Jiang, Q. Effect of alloying elements on microstructure and properties of multiprincipal elements high-entropy alloys. *J. Alloy. Compd.* **2009**, *475*, 752–757. [CrossRef]

64. Schuh, B.; Mendez-Martin, F.; Völker, B.; George, E.; Clemens, H.; Pippan, R.; Hohenwarter, A. Mechanical properties, microstructure and thermal stability of a nanocrystalline CoCrFeMnNi high-entropy alloy after severe plastic deformation. *Acta Mater.* **2015**, *96*, 258–268. [CrossRef]

65. Wang, X.; Zhang, Y.; Qiao, Y.; Chen, G. Novel microstructure and properties of multicomponent CoCrCuFeNiTi$_x$ alloys. *Intermetallics* **2007**, *15*, 357–362. [CrossRef]

66. Zhang, K.B.; Fu, Z.Y.; Zhang, J.Y.; Wang, W.M.; Wang, H.; Wang, Y.C.; Zhang, Q.J. Characterization of nanocrystalline CoCrFeNiCuAl high-entropy alloy powder processed by mechanical alloying. *Mater. Sci. Forum* **2009**, *620*, 383–386. [CrossRef]

67. Zhou, Y.; Zhang, Y.; Kim, T.; Chen, G. Microstructure characterizations and strengthening mechanism of multi-principal component AlCoCrFeNiTi$_{0.5}$ solid solution alloy with excellent mechanical properties. *Mater. Lett.* **2008**, *62*, 2673–2676. [CrossRef]

68. Zhou, Y.; Zhang, Y.; Wang, F.; Chen, G. Phase transformation induced by lattice distortion in multiprincipal component CoCrFeNiCu$_x$Al$_{1-x}$ solid-solution alloys. *Appl. Phys. Lett.* **2008**, *92*, 241917. [CrossRef]

69. Takeuchi, A.; Inoue, A. Quantitative evaluation of critical cooling rate for metallic glasses. *Mater. Sci. Eng. A* **2001**, *304*, 446–451. [CrossRef]

70. Takeuchi, A.; Inoue, A. Classification of bulk metallic glasses by atomic size difference, heat of mixing and period of constituent elements and its application to characterization of the main alloying element. *Mater. Trans.* **2005**, *46*, 2817–2829. [CrossRef]

71. Miedema, A.; de Chatel, P.; de Boer, F. Cohesion in alloys—Fundamentals of a semi-empirical model. *Physica B C* **1980**, *100*, 1–28. [CrossRef]

72. Hammond, V.H.; Atwater, M.A.; Darling, K.A.; Nguyen, H.Q.; Kecskes, L.J. Equal-channel angular extrusion of a low-density high-entropy alloy produced by high-energy cryogenic mechanical alloying. *JOM* **2014**, *66*, 2021–2029. [CrossRef]

73. Benjamin, J.S. Dispersion strengthened superalloys by mechanical alloying. *Metall. Trans.* **1970**, *1*, 2943–2951.

74. Stepanov, N.; Shaysultanov, D.; Salishchev, G.; Tikhonovsky, M. Structure and mechanical properties of a light-weight AlNbTiV high entropy alloy. *Mater. Lett.* **2015**, *142*, 153–155. [CrossRef]

75. Zardiackas, L.D.; Parsell, D.E.; Dillon, L.D.; Mitchell, D.W.; Nunnery, L.A.; Poggie, R. Structure, metallurgy, and mechanical properties of a porous tantalum foam. *J. Biomed. Mater. Res.* **2001**, *58*, 180–187. [CrossRef]

76. Lefebvre, L.-P.; Banhart, J.; Dunand, D. Porous metals and metallic foams: Current status and recent developments. *Adv. Eng. Mater.* **2008**, *10*, 775–787. [CrossRef]

77. Čapek, J.; Vojtěch, D. Effect of sintering conditions on the microstructural and mechanical characteristics of porous magnesium materials prepared by powder metallurgy. *Mater. Sci. Eng. C* **2014**, *35*, 21–28. [CrossRef] [PubMed]

78. Kang, M.-H.; Jung, H.-D.; Kim, S.-W.; Lee, S.-M.; Kim, H.-E.; Estrin, Y.; Koh, Y.-H. Production and bio-corrosion resistance of porous magnesium with hydroxyapatite coating for biomedical applications. *Mater. Lett.* **2013**, *108*, 122–124. [CrossRef]

79. Čapek, J.; Vojtěch, D. Properties of porous magnesium prepared by powder metallurgy. *Mater. Sci. Eng. C* **2013**, *33*, 564–569. [CrossRef] [PubMed]

80. Cay, H.; Xu, H.; Li, Q. Mechanical behavior of porous magnesium/alumina composites with high strength and low density. *Mater. Sci. Eng. A* **2013**, *574*, 137–142. [CrossRef]

81. German, R.M. *Powder Metallurgy Science*; Metal Powder Industries Federation: Princeton, NJ, USA, 1984.

82. Schaffer, J.P.; Saxena, A.; Antolovich, S.D.; Sanders, T.; Warner, S.B. *The Science and Design of Engineering Materials*; MacGraw-Hill Irwin: Chicago, IL, USA, 1995.

83. Gupta, M.; Wong, W. Enhancing overall mechanical performance of metallic materials using two-directional microwave assisted rapid sintering. *Scr. Mater.* **2005**, *52*, 479–483. [CrossRef]

84. Hashmi, S. *Comprehensive Materials Processing*; Elsevier: Burlington, MA, USA, 2014.

85. Gupta, M.; Lai, M.; Soo, C. Processing-microstructure-mechanical properties of an Al-Cu/SiC metal matrix composite synthesized using disintegrated melt deposition technique. *Mater. Res. Bull.* **1995**, *30*, 1525–1534. [CrossRef]

86. Subramanian, J.; Guan, K.C.; Kuma, J.; Gupta, M. Feasibility study on utilizing carbon dioxide during the processing of Mg-Al alloys. *J. Mater. Process. Technol.* **2011**, *211*, 1416–1422. [CrossRef]

87. Sankaranarayanan, S.; Jayalakshmi, S.; Gupta, M. Effect of addition of mutually soluble and insoluble metallic elements on the microstructure, tensile and compressive properties of pure magnesium. *Mater. Sci. Eng. A* **2011**, *530*, 149–160. [CrossRef]

88. Shanthi, M.; Gupta, M.; Jarfors, A.; Tan, M. Synthesis, characterization and mechanical properties of nano alumina particulate reinforced magnesium based bulk metallic glass composites. *Mater. Sci. Eng. A* **2011**, *528*, 6045–6050. [CrossRef]

89. Gupta, M.; Lai, M.; Saravanaranganathan, D. Synthesis, microstructure and properties characterization of disintegrated melt deposited Mg/SiC composites. *J. Mater. Sci.* **2000**, *35*, 2155–2165. [CrossRef]

90. Hassan, S.; Gupta, M. Development of ductile magnesium composite materials using titanium as reinforcement. *J. Alloy. Compd.* **2002**, *345*, 246–251. [CrossRef]

91. Ho, K.; Gupta, M.; Srivatsan, T.S. The mechanical behavior of magnesium alloy AZ91 reinforced with fine copper particulates. *Mater. Sci. Eng. A* **2004**, *369*, 302–308. [CrossRef]

92. Nguyen, Q.; Gupta, M. Enhancing compressive response of AZ31B magnesium alloy using alumina nanoparticulates. *Compos. Sci. Technol.* **2008**, *68*, 2185–2192. [CrossRef]

93. Paramsothy, M.; Hassan, S.; Srikanth, N.; Gupta, M. Enhancing tensile/compressive response of magnesium alloy AZ31 by integrating with Al_2O_3 nanoparticles. *Mater. Sci. Eng. A* **2009**, *527*, 162–168. [CrossRef]

94. Meenashisundaram, G.K.; Gupta, M. Low volume fraction nano-titanium particulates for improving the mechanical response of pure magnesium. *J. Alloy. Compd.* **2014**, *593*, 176–183. [CrossRef]

95. Meenashisundaram, G.K.; Seetharaman, S.; Gupta, M. Enhancing overall tensile and compressive response of pure Mg using nano-TiB_2 particulates. *Mater. Charact.* **2014**, *94*, 178–188. [CrossRef]

96. Ng, C.; Savalani, M.; Man, H.; Gibson, I. Layer manufacturing of magnesium and its alloy structures for future applications. *Virtual Phys. Prototyp.* **2010**, *5*, 13–19. [CrossRef]

97. Savalani, M.; Hao, L.; Harris, R.A. Evaluation of CO_2 and Nd: YAG lasers for the selective laser sintering of HAPEX®. *J. Eng. Manuf.* **2006**, *220*, 171–182. [CrossRef]